Delft University of Technology

Field Test and Numerical Study of Train-Induced Vibration of Over-Track Buildings Above Metro Depot

Chen, Zhaowei; Wan, Fangshuang; He, Chunyan

Important note
To cite this publication, please use the final published version (if applicable).
Please check the document version above.

Field Test and Numerical Study of Train-Induced Vibration of Over-Track Buildings Above Metro Depot

Zhaowei Chen[1] · Fangshuang Wan[1] · Chunyan He[2]

Abstract To maximize the use of urban land, many cities have built buildings above metro depots. However, the low-frequency vibration caused by metro operation affects the lives of surrounding residents, which seriously restricts the further development of over-track buildings. To study this problem, Firstly, the vibration of the metro depot and surrounding sensitive areas are tested on a large actual metro depot in Southwest China, and the rail, sleeper/support column, bearing column, and cover plate are mainly tested. Then, considering nonlinear factors such as mechanical properties of building materials, soil layering characteristics, and artificial viscoelastic boundary, the numerical coupled model of the train-track-depot-building is established, and the simulation data are compared with the test data to verify the accuracy of the numerical model. Finally, the impact of metro operation on the over-track buildings is evaluated. Results show that for the over-track buildings concerned in this paper, the floor vibration near the rail is the strongest, the main vibration frequency of the office building is concentrated in 10–20 Hz, and the maximum Z vibration level (VL_{zmax}) of the office building is 52.02 dB. The main vibration frequency of the residential building is similar to that of the office building, and the superposition of floor vibration energy causes the vibration of the mid-span point to be larger than the vibration of the corner point and the side wall point. The vibration wave of lower floors mainly propagates through the bearing column, and the vibration of the parking garage is larger than other buildings. The research results can provide a reference for the vibration control and design of over-track buildings above the metro depot.

Keywords Metro depot · Vehicle-track coupled dynamics · Field test · Low-frequency vibration · Over-track buildings

1 Introduction

To maximize the use of land resources in China's urban centers, the development model of over-track buildings oriented by public transportation came into being. But metro operations cause vibration waves that are transmitted to the ground, and the soil-building coupled will cause the building vibration, which directly affects the daily life of the upper residents [1]. This problem has also become a key factor restricting the development of the property complex covered by the metro depot. In addition, the large metro depot contains many track lines and the upper area is planned to construct buildings of different functional types, and the vibration propagation characteristics are diverse. Research on the vibration response of over-track buildings above depot needs to be enhanced.

Some researchers have studied the building vibration caused by the metro. According to the different research methods, the vibration problems of buildings caused by metro can be divided into three types: (1) Field test: Liang et al. [2] measured the building vibration, and the analysis of the correlation between natural frequency and environmental vibration frequency of the building was carried out. Chen et al. [3] conducted a field test in the underground depot and found that the linear attenuation rate of the train in the edge

✉ Chunyan He
   3812412099@qq.com

1 School of Mechanotronics and Vehicle Engineering, Chongqing Jiaotong University, Chongqing 400074, China

2 Section of Railway Engineering, Delft University of Technology, Stevinweg 1, 2628 CN Delft, The Netherlands

area of the track was about 0.2 dB / m. Zhang et al. [4] tested track 11 line in Shanghai, China, and studied the measurement results of tunnel and ground vibration. Zhang et al. [5] analyzed the influence of duxseal material on vibration reduction and researched the vibration difference between duxseal lining and traditional lining through field test vibration data. Shao et al. [6] analyzed the influence of building vibration, and the vibration and noise of metro depot were analyzed. Di et al. [7] researched the vibration level of the building floor the basement and the basement through the field test of the building vibration above the metro. Cao et al. [8] carried out vibration tests on residential building at the metro depot to study the frequency spectrum and acceleration time history at different locations. (2) Numerical simulation: Tao et al. [9] studied metro-induced vibration transmission in buildings using finite elements. Zhang et al. [10] used a numerical model to analyze the ground vibration by metro operation on elevated bridges. Chen et al. [11] established a numerical coupled model using the finite element method and found that the wave-impeding block can effectively control low-frequency vibration. Ling et al. [12] proposed a high-precision Caughey damping numerical modeling technology for metro cover and studied the effect of metro operation on residents ' comfort. Xiong et al. [13] put forward a tunnel finite element model and compared the effects of different vibration sources. Zou et al. [14] established the numerical model and the different wave barriers were studied for their vibration isolation effects. Ling et al. [15] established the numerical model, and the train-induced building vibration was analyzed. Chen et al. [16] analyzed the seismic performance and damage mechanism of metro station using the finite element model. (3) Theoretical analysis: Kouroussis et al. [17] predicted train-induced ground vibrations using transfer functions. Cao et al. [18] established the response transfer function (RTF) of the building by wave analysis method and studied the vibration level of the buildings. Mouzakis et al [19] used transfer function (TF) to study the vibration transfer law of the metro. Wang et al. [20] used different algorithms to study the transfer characteristics from the target environment and the vibration source. Li et al. [21] proposed OTPA and SVD formulas to predict the vibration of building. Ma et al. [22] studied the vibration influence of this function on optimizing periodic piles using band gap performance evaluation function. The above research proposes a variety of solutions for the vibration problem caused by train, but the target over-track buildings of the research are relatively simple. Currently, most research focuses on the vibration propagation law of the vibration wave on different floors of the over-track buildings, while ignoring the vibration response differences of different rooms on the same floor and different locations in the same room. The types of train vibration sources are more complex and diverse in the depot area (especially in the throat area),

and the research on different architectural functional areas covered by the depot is rarely reported. Therefore, it would be useful to continue vibration research on the over-track buildings above depot.

To evaluate the influence of metro operation on low-frequency vibration of over-track buildings, this paper takes a large depot project in Chongqing, China. The vibration acceleration of the metro depot and surrounding sensitive areas are tested. Through the field test, the vibration data of the metro depot is obtained. Considering nonlinear factors such as mechanical properties of building materials, soil layering characteristics, and artificial viscoelastic boundary, the numerical coupled model of train-track-soil-building is established. To verify the model's accuracy, the simulation data is compared with the test data. On this basis, the effect of the collision between the wheelset and the turnout switch rail in the throat area is considered, compare the vibration differences between the non-turnout area and the turnout area and the impact of the metro operation on the proposed buildings are systematically evaluated.

2 Field Test of Metro Depot

This paper studies the property project of a large metro depot, mainly conducting vibration testing on the over-track area, parking area, and throat area, respectively. The test data can provide data support for the reliability verification of the numerical model.

2.1 Practical Engineering

The property project on the top of the proposed large metro depot is located in Chongqing, China, the east-west width of the depot is about 190 m, and the north-south length is about 750 m. As shown in Fig. 1, the project includes 6 office buildings and 12 high-rise residential buildings, and the residential building on the right is located directly above the parking track L2 line.

2.2 Field Test

The test line is a track L2 line, and the test trains are six-car unit as-type metro trains. The vibration acceleration of rail, sleeper/support column, bearing column, and over plate are measured respectively, and the overall change trend, frequency distribution, and peak frequency of acceleration in the longitudinal plane (along the track direction) and vertical plane are compared, the transmission law and time-frequency characteristics of vibration are analyzed.

2.2.1 Evaluation Criteria

Based on the standards of "Standards for building vibration induced by urban rail transit and secondary radiation noise (JGJT170-2009)", the high-rise residential and office building planned by the project belong to "residential, cultural and educational areas". The standard limit of 62 dB at night and 65 dB during the day is implemented for the vibration acceleration level.

2.2.2 Test Instrument

The vibration testing equipment mainly includes the ICP acceleration sensor and INV3062SC intelligent acquisition instrument, as shown in Fig. 2.

INV3062SC intelligent acquisition instrument is used for dynamic data acquisition, and all input channels are sampled synchronously. The property of the sensor is shown in Table 1, the ICP acceleration sensor is used to pick up vibration signals, and the transverse sensitivity of the instrument is all less than 5%.
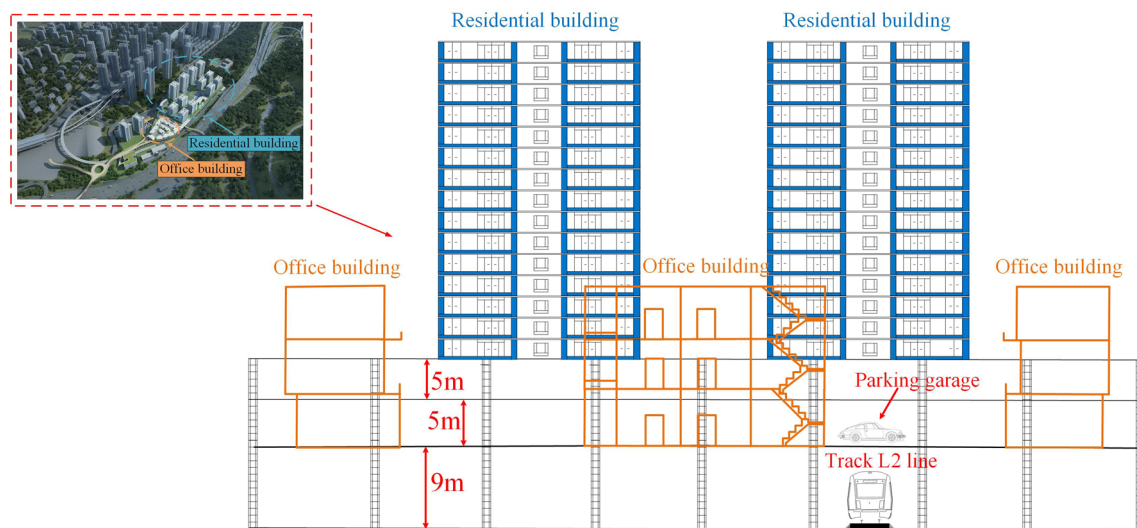

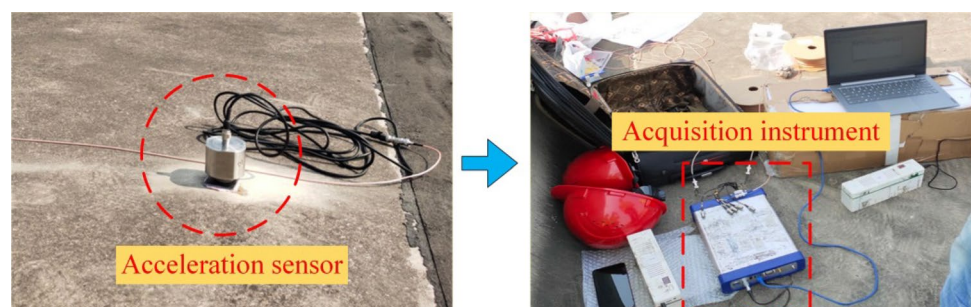**Fig. 1** Overview of metro depot

Fig. 2 Experiment equipment

Table 1 Property of sensor

Test position	Instrument type	Charge sensitivity (mv/g)	Frequency range (Hz)	Sampling frequency (Hz)
Rail	NV9822	100	0.2–8000	2048
Sleeper/support column	CT11000L	10000	0.2–500	1000
Cover plate	LC0132T	50000	0.05–500	2048
Bearing column	LC0106T	1000	0.05–1500	2048

2.2.3 Test Scheme

As shown in Fig. 3, in this test, three test sections are selected on the track L2 line, and the spacing of each test section is about 100 meters. Test section 1 is arranged in the throat area, and test sections 2 and 3 are arranged in the parking area. Vibration levels are higher in the vertical vibration caused by train than in the longitudinal and lateral vibration [23]. Therefore, vertical vibration acceleration is tested in this paper. The test points of the vertical section mainly include rail acceleration A, sleeper/support column acceleration B, bearing column acceleration C, and cover plate acceleration D, as shown in Fig. 4.

2.3 Data Analysis

As shown in Fig. 5, from test section 1 to test section 3, the vibration acceleration of the sleeper/support column is notably reduced. The peak acceleration of the sleeper test point 1 in the throat area is 11 m/s^2, while the peak acceleration of the support column test point 3 in the parking area is only 0.5 m/s^2. The reason is the influence of the collision between the wheelset and the turnout switch rail, Due to the influence of the collision between the turnout switch rail and the wheelset, hence the vibration level of the throat area is obviously larger than that of the parking area. At the support column test point 2, the acceleration amplitude increases sharply at 100 s, the reason is that the train is passing through the rail turnout. At the support column test point 3, the time-domain curve of the first half is the metro passes through the throat area, and the time-domain curve of the second half is the metro passes through the parking area. There is a parking whistle when the metro runs between the throat area and the parking area, resulting in the acceleration amplitude tending to zero.

The vibration acceleration level of the cover plate is consistent with that of the bearing column, as shown in Fig. 6. The VL$_{zmax}$ of the bearing column is 54.3 dB in three test sections, and the main vibration frequency of the sleeper is concentrated in 50–80 Hz. The VL$_{zmax}$ of the rail are 103.19, 102.78, and 94.41 dB, respectively. The vibration energy attenuation along the track direction is relatively slow.

As shown in Fig. 7, the VL$_{zmax}$ is the maximum Z vibration level, and the A_{max} is the maximum acceleration.
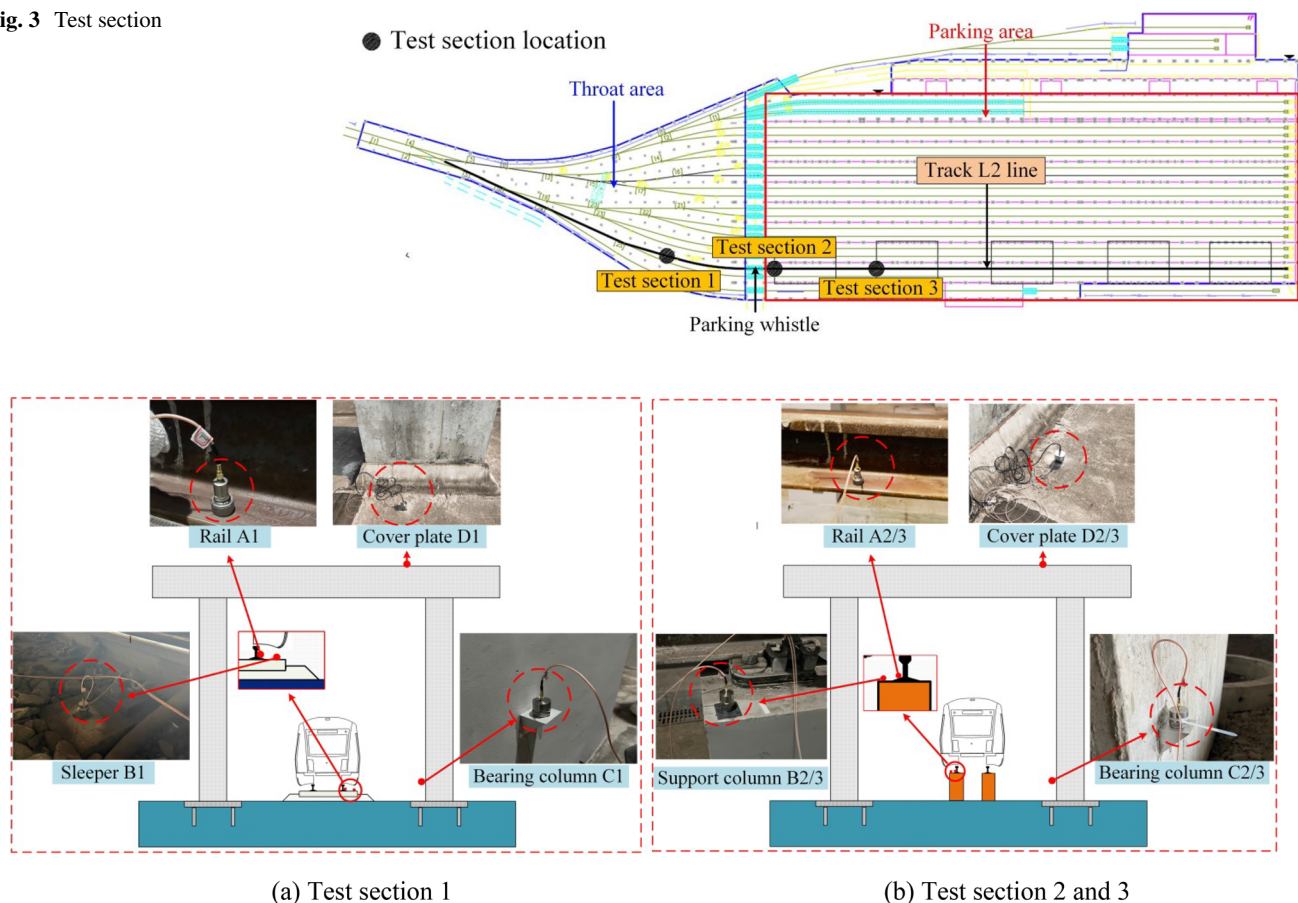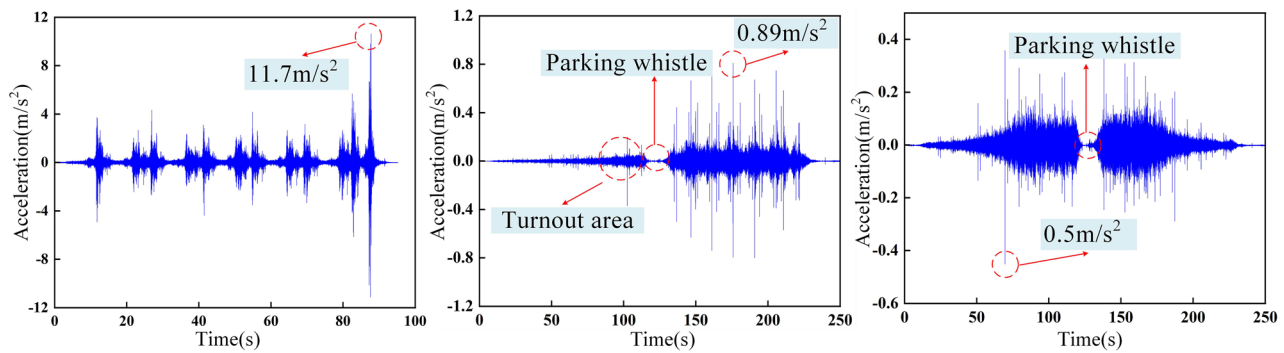

Fig. 3 Test section

Fig. 4 Location of testing point

(a) Test section 1

(b) Test section 2 and 3

Fig. 5 Sleeper/support column in time domain

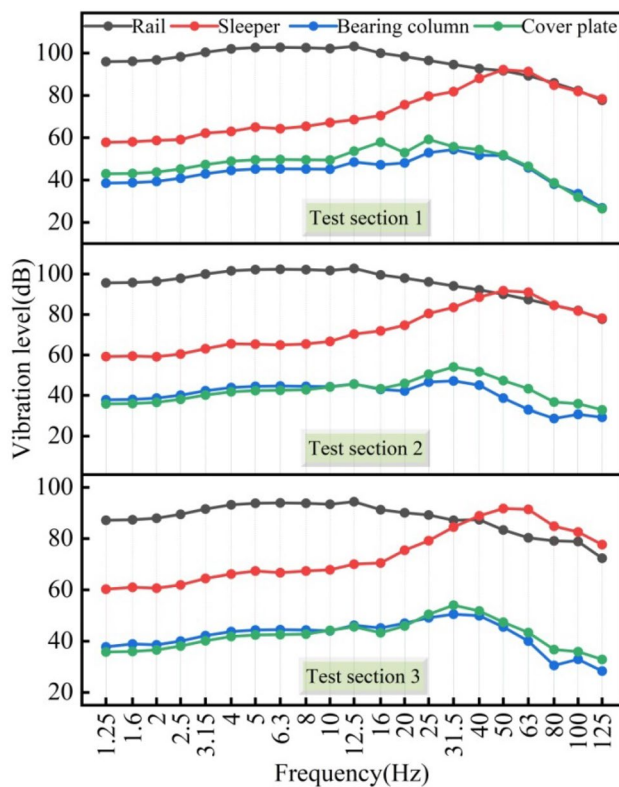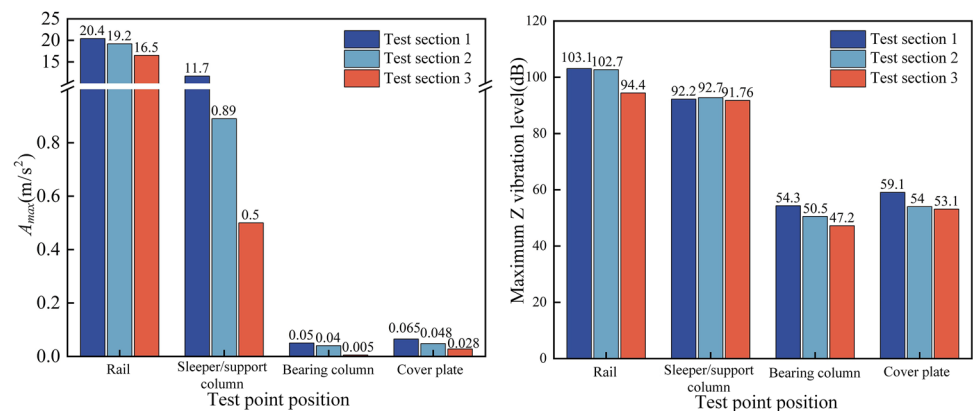**Fig. 6** One-third octave frequency of testing point

From the perspective of the longitudinal plane, the maximum acceleration of rail A1 is 20.4 m/s², and the peak acceleration of rail A1 to A3 decreases by 3.9 m/s². The vibration acceleration of the sleeper/support column decreased significantly from test point 1 to test point 3. The maximum acceleration is located at D1 in the cover plate, and the VL_{zmax} of the cover plate is 59.1dB.

From the vertical plane, the acceleration attenuation from the rail to the bearing column is large, and the vibration acceleration decreases by 20 m/s². The vibration level of the bearing column is close to that of the cover plate. The VL_{zmax} at the A1 position is 103.1 dB, while the VL_{zmax} at the C1 position is only 54.3 dB, and the attenuation rate is 50%. The vibration of the cover plate is within the standard limit.

3 Vibration Prediction Numerical Models

The vibration waves generated by the collision between the wheelset and the rail are transmitted to the ground, which will influence the stability of the over-track buildings. Hence through the establishment of the numerical prediction model, the impact of the metro operation on the over-track buildings is evaluated.

Fig. 7 Tested data

3.1 Research Method

As shown in Fig. 8, the research method flow chart of the over-track building's vibration has been listed. Firstly, the train sub-models and track sub-models are established based on multibody dynamics theory and Euler beam vibration theory respectively. Considering the elastic deformation between wheel and rail, the stochastic track irregularity is calculated by using the American grade 5 irregularity spectral density function and random irregularity of short wave. The train-track coupled causes train vibration, rail vibration, and sleeper vibration, and the next step is to extract the fastener force. By using ANSYS, the numerical prediction model is established. To verify the accuracy of the model, simulation data are compared with test data. Then, loaded to the monolithic track bed by fastening force as excitation,

and then vibration propagates upward through soil-building coupled. Finally, the vibration level of the train-induced over-track buildings is further analyzed.

3.2 Train-Track Coupled Dynamic Model

Considering the incentive mechanism of track irregularity and the interaction of train, rail, sleeper, and track bed, based on the multi-body dynamics theory proposed by Zhai [24], the train-track coupled dynamics model is established. As shown in Fig. 9, the vertical unified model of the vehicle-track has been established, and the main dynamic model notations are shown in Table 2.

Based on the theory of multibody dynamics, a six-car unit as-type metro train is placed equally spaced at certain intervals, and each carriage is considered to be
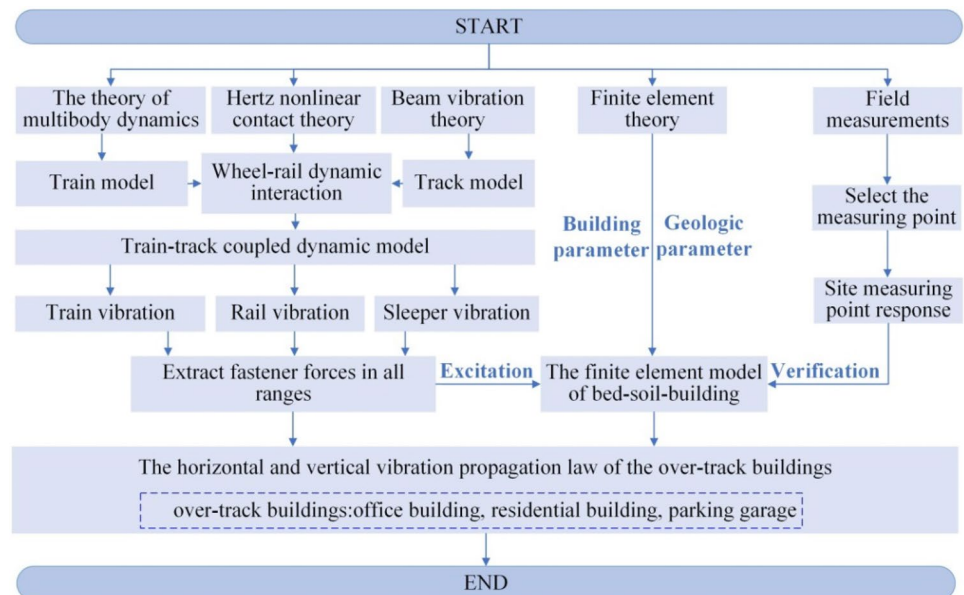

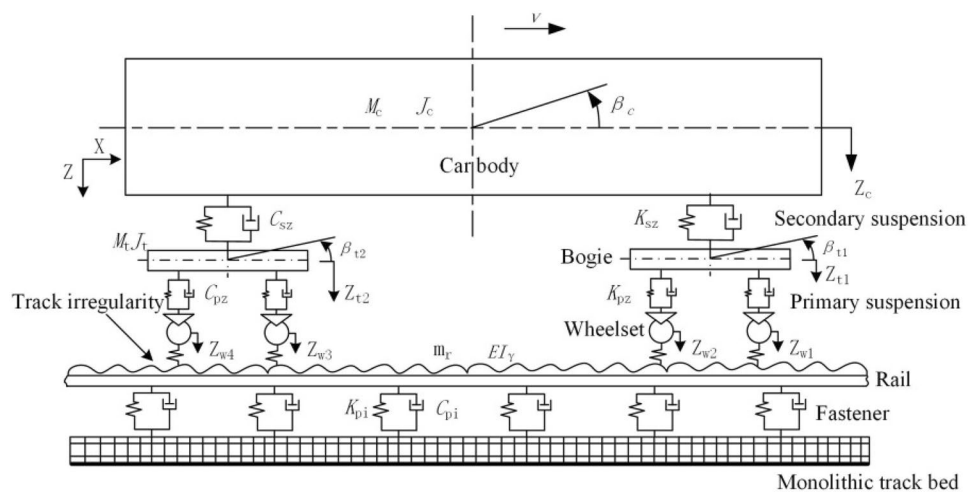**Fig. 8** Research method flow chart

Fig. 9 Diagram of train-track model

Table 2 Train-track model parameters

Symbol	Physical meaning
Z_t, Z_c, Z_w	Vertical displacement of frame, carbody and wheelset
J_c, J_t	Nodal inertia of carbody and frame
K_{sz}, K_{pz}	Secondary and primary suspension stiffness
C_{sz}, C_{pz}	Secondary and primary suspension damping
M_t, M_c, M_w	Frame, carbody and wheelset mass
β_c, β_t	Carbody, frame nodding angle
g	Acceleration of gravity
m_r	Unit length mass of rail
EI_γ	Bending stiffness of rail
C_{pi}, K_{pi}	Damping and stiffness of track cushion corresponding

Table 3 Vehicle dynamics index

Carbody parameter	Numerical value	Unit
Train formation	6	–
Train speed	15	km/h
Bicycle size	$22 \times 3.0 \times 3.8$	m
Body mass (empty car)	22.7	t
Frame nod inertia	1.47	t/m²
Frame quality	4.28	t
Bogie wheelbase	2.5	m
Wheelset mass	1.86	t
Vehicle spacing	15.7	m
Body nodding inertia	1959	t/m²

a multi-rigid body structure. Each carriage of an as-type train is composed of four wheelsets, two frames, and one carbody, the elastic deformation of each rigid body element is not considered. Each rigid body element is connected by elastic suspension elements. The pitch motion and bounce motion of the frame and frame carbody are considered, and the vertical motion of the wheelset is considered. So the degree of freedom of the whole vehicle subsystem is 10, the kinetic equation can be seen in the published literature [25]. The main vehicle index is shown in Table 3.

The matrix form for each vehicle in the time domain can be expressed as:

$$M_V \ddot{Z}_V + C_V(\dot{Z}_V)\dot{Z}_V + K_V(Z_V)Z_V = F_v(Z_V, Z_T, \dot{Z}_V, \dot{Z}_T) + F_{EXT} \tag{1}$$

In the equation, the track displacement and vehicle displacement are represented by Z_T and Z_V, respectively. The stiffness matrix and damping matrix are represented by K_V and C_V, respectively. F_V is a load vector derived from the displacement of the vehicle and tracks, and M_V is the vehicle mass. F_{EXT} is the external forces, including gravity and the external forces generated by the centripetal

acceleration through the curved track. The Wheel-rail contact determines the coupled relationship between turnout and vehicle.

$$p(t) = \left[\frac{1}{G}\Delta Z(t)\right]^{3/2} \tag{2}$$

In the equation, and the wheel-rail contact constant and the wheel-rail force are represented by G and $p(t)$, respectively. $\Delta Z(t)$ is the elastic compression between rail and wheel.

$$\begin{cases} \Delta Z(t) = Z_w(t) - Z_r(t) \\ G = 4.57R^{-0.149} \times 10^{-8} \\ \sigma(t) = S[p(t)]^{1/3} \\ S = 2.49R^{-0.251} \times 10^7 \end{cases} \tag{3}$$

In the equation, the vertical displacement of the wheel and the rail are represented by $Z_w(t)$ and $Z_r(t)$, respectively. The stress constant and the wheel-rail contact stress are represented by S and $\sigma(t)$, respectively, and R is the wheel radius. When $\Delta Z(t)$ is less than or equal to 0, it shows the rail has been derailed, and the $p(t)$ is equal to 0. When there is a displacement irregularity between the rail and wheel, then Eq. (2) can be changed into the following equation:

$$\begin{cases} p(t) = 0 & \Delta Z(t) \le 0 \\ p(t) = \left\{\frac{1}{G}\left[\Delta Z_w(t) - Z_1(t) - Z_0(t)\right]\right\}^{3/2} & \Delta Z(t) > 0 \end{cases} \tag{4}$$

The specific vehicle-turnout system coupling model and numerical calculation are shown in the reference [26]. For the track model including track bed, sleeper, fastener, and rail, considering the effect of the boundary conditions of rail vibration. Using the Euler beam to simulate the track, the shear deformation is not considered, and only the bending deformation of the rail is considered, which mainly ensures sufficient numerical accuracy. Using elastic spring damping element to simulate fasteners, and the spring force depends on the difference between the displacement of the rails and the displacement of the track bed (extracted by the finite element model) [27].

According to the explicit integral method proposed by Zhai [28], the system dynamics equation is solved. As shown in Fig. 10, the fastener force is solved by numerical integration iteration.

3.3 Finite Element Model of Over-Track Buildings

The numerical model of track bed-soil-building is established by using ANSYS, as shown in Fig. 11, and the following principles are followed in the specific modeling process:
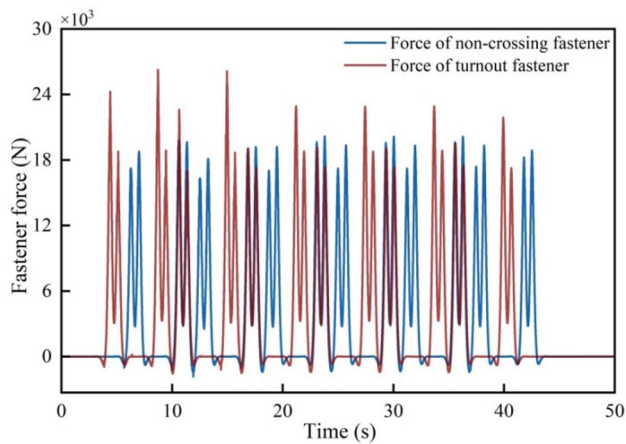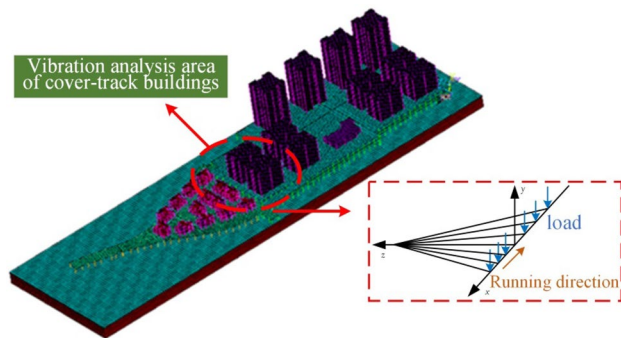
Fig. 10 Fastener force

Fig. 11 Finite element model

(1) Using Timoshenko beam theory, the cover plate struts and building struts are modeled using BEAM188 beam elements (BEAM188: A three-dimensional elastic beam unit that can withstand tension, pressure, bending, and torsion, including 2 nodes, each node has the translation and the rotation of x, y, and z in three axes). SHELL63 shell unit is used to build the cover plate floor and building floor (SHELL63: shell unit that can bear the load in the plane and normal direction, including 4 nodes, each node has the translation and the rotation of x, y, and z in three axes). The solid unit SOLID45 is used to build the integral track bed and soil

(SOLID45: used to build the solid structure, consisting of 8 nodes, each node has the translation of x, y, and z in three axes).

(2) Considering the track bed as the foundation structure in the numerical model, the fastener force is loaded into the monolithic track bed as the excitation force [25].

(3) The finite element model after grid division contains 22228649 nodes and 1997688 elements. Considering the large number of nodes and elements, the solving process takes a long time, and it needs to be solved numerically with the help of high-performance workstations.

(4) To ensure sufficient calculation accuracy, the time of implicit integration should be less than or equal to 1/100 of the system's maximum period, so the integral step is 0.002 s to meet the frequency requirement of 200 Hz.

$$\Delta t \leq \frac{T_{\max}}{100} = \frac{1}{100 f_{\min}} \tag{5}$$

(5) The propagation speed of vibration waves is 2400 m/s in reinforced concrete [29], the main vibration frequency of buildings caused by metro does not exceed 100 Hz, and the calculated minimum shear wavelength of vibration waves in buildings is 24 m. When the distance between the model boundary and the load position is larger than half of the maximum wavelength of soil, the calculation accuracy is ensured. Therefore, the grid sizes of column element, plate element, and beam element are divided into 0.5, 0.6, and 0.5 m, respectively. According to the soil material parameters, the grid size of soil elements is divided into 0.3 m. The material main parameter of soil is shown in Table 4.

(6) To reduce the vibration reflection effect of the boundary, it is important to set a layer of three-dimensional equivalent uniform viscoelastic boundary [30]. The equations and parameters of the artificial boundary are as follows:

$$\begin{cases} \text{Tangential boundary} : C_{BT} = \rho c_s, K_{BT} = \alpha_T \frac{G}{R} \\ \text{Normal boundary} : C_{BN} = \rho c_P, K_{BN} = \alpha_N \frac{G}{R} \end{cases} \tag{6}$$

Table 4 Soil parameters

Soil type	Depth (m)	Density (g/cm³)	Elastic modulus (MPa)	Poisson ratio
Plain fill	0–2	1.75	51	0.401
Clay	2–4	1.96	173	0.372
Fully weathered hard mudstone	4–9	2.05	385	0.348
Strongly weathered hard mudstone	9–16	2.3	4036	0.315
Medium weathered hard mudstone	Over 16	2.51	6490	0.282

In the equation, the coefficient of the spring and damping is represented by K_B and C_B, respectively, and α is the artificial boundary parameter. The soil density and the shear modulus are represented by ρ and G, respectively. The distance between the boundary point vibration source and vibration source and the wave velocity are represented by R and c, respectively.

$$\begin{cases} \tilde{G} = \alpha_T h \frac{G}{R} \\ \tilde{E} = \alpha_N h \frac{G}{R} \cdot \frac{(1+\tilde{v})(1-2\tilde{v})}{(1-\tilde{v})} \\ \eta = \frac{\rho R}{3G}\left(2\frac{v_S}{\alpha_T} + \frac{v_P}{\alpha_N}\right) \\ \tilde{v} = \begin{cases} \dfrac{\alpha-2}{2(\alpha-1)}, \alpha > 2 \\ 0, \qquad\quad \text{other} \end{cases}, \alpha = \frac{\alpha_N}{\alpha_T} \end{cases} \tag{7}$$

In the equation, the damping ratio, the shear modulus, and the elastic modulus are represented by η, $\tilde{G}$, and $\tilde{E}$. respectively. The soil's compression wave velocity and the soil's shear wave velocity are represented by v_p and v_s, respectively. $\tilde{v}$ is the equivalent Poisson, h is the thickness, and α is the equivalent parameter. The tangential artificial boundary parameters α_T and normal artificial boundary parameters α_N are 0.67 and 1.33 respectively.

3.4 Model Validation

As shown in Fig. 12, the vibration acceleration level of the sleeper test point 1, the bearing column test point 2, and the cover plate test point 3 are compared, respectively. Simulation data are basically consistent with test data in terms of frequency distribution, and only a small part of the frequency domain is different, mainly due to the deviation between the building materials in the numerical model and the actual working conditions, which is slightly different. In general, the test results are basically consistent with the

simulation results, which indicate the numerical model's accuracy.

4 Horizontal Vibration of Over-Track Buildings

This chapter mainly studies the time-frequency analysis of horizontal vibration of office building, residential building, and parking garages. Compare the environmental vibration limits of urban areas to evaluate the overall vibration impact of over-track buildings.

4.1 Horizontal Vibration of Office Building

As shown in Fig. 13, the vibration level of the mid-span point, side wall point, and corner point of the office building room are compared, respectively, and the vibration propagation law of different positions on the same floor is analyzed.

The vibration level of the mid-span point "B" in the three rooms is the largest, as shown in Fig. 13b, and it shows that the larger room will cause more vibrations on the floor. Compared with the acceleration of the same room, the vibration acceleration of the mid-span point "B" is significantly larger than the corner point "E" and the side wall point "D". The reason is that the vibration wave around the wall in the same closed room is transmitted to the mid-span point, the vibration wave energy is superimposed, and the stiffness of the mid-span point is less than that of the side wall point and the corner point.

The vibration level of the mid-span point in the same room is the largest, the main vibration frequency of the floor is between 10 Hz and 31.5 Hz, and the VL_{zmax} of the office building is 52.02 dB in 12.5 Hz, as shown in Fig. 13c. Based on the above standards, the residential buildings' vibration is within the standard limit, and it shows that the level over-track building vibration belongs to low-frequency micro-vibration.
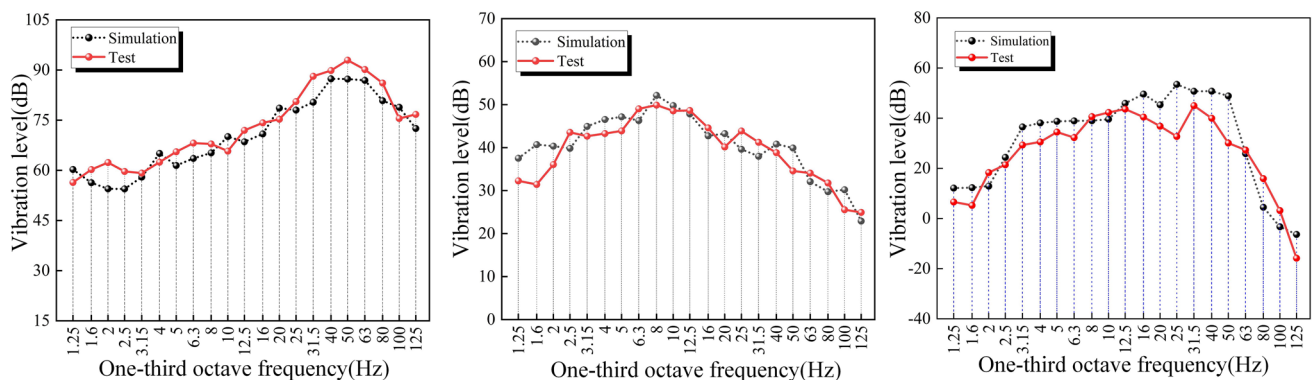

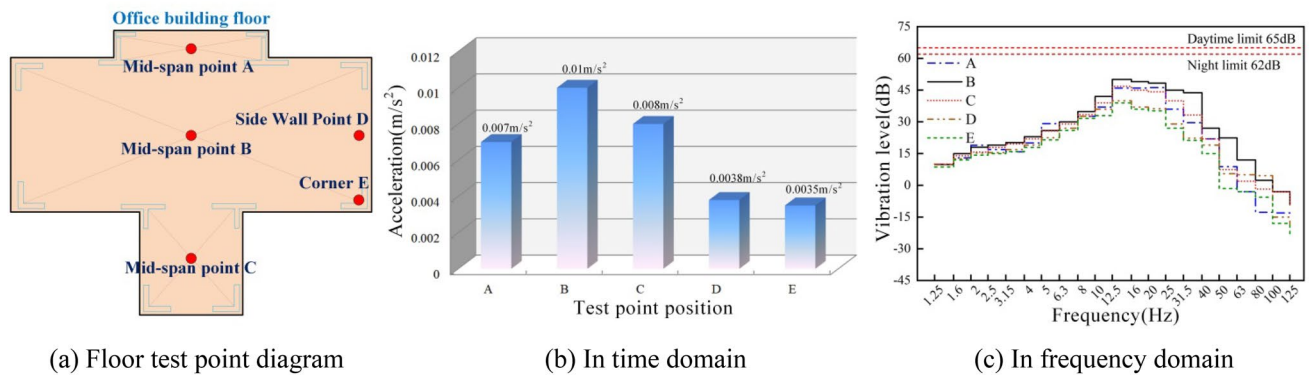**Fig. 12** Frequency domain comparison diagram

(a) Floor test point diagram   (b) In time domain   (c) In frequency domain

Fig. 13 Comparison of horizontal vibration of office building

4.2 Horizontal Vibration of Residential Building

As shown in Fig. 14, the above research office building room vibration differences in different positions, to further analyze the lateral vibration propagation law of the residential building, eight mid-span positions of different rooms on the first floor of the office building are selected for vibration analysis. The peak acceleration of the test points "N4" and "N5" is 0.005 m/s^2, and the acceleration amplitude decreases with increasing distance between the track L2 line and the test point.

4.3 Horizontal Vibration of Parking Garage

From the horizontal plane, the vibration level of the mid-span point position and the column point position of the negative second floor in the parking garage are compared in Fig. 15.

The vibration of the column point in the parking garage is larger than that of the mid-span point. The peak acceleration of the column point position is 0.016 m/s^2, and the peak acceleration of the mid-span point position is only 0.01 m/s^2, which is attenuated by 0.006 m/s^2. The vibration response
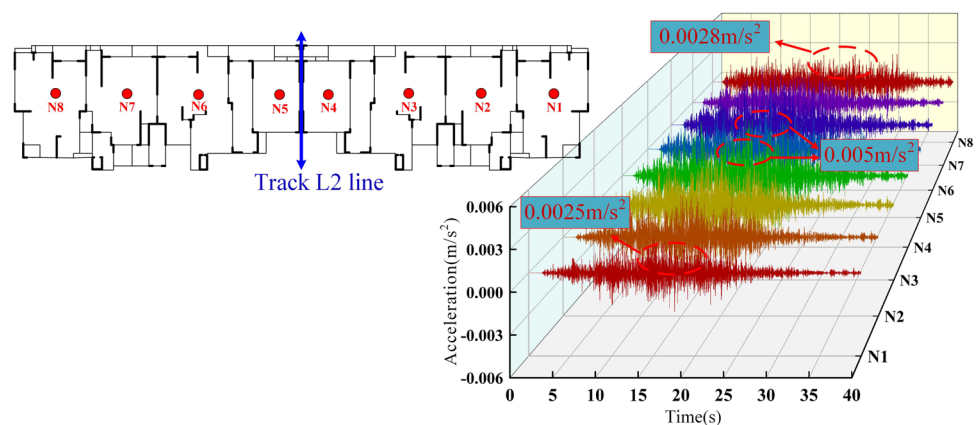
change trend of the column point and the mid-span point is basically the same. The horizontal vibration of the parking garage is no vibration exceeding the standard limit. *The VL_{zmax} of the column point is 59 dB, and the VL_{zmax} of the mid-span point is 50 dB.* Due to the parking garage is close to the track, the vibration wave propagates mainly through the bearing column, and the vibration at the column point is greater than that at the mid-span point.

4.4 Comparison of Horizontal Vibration of Over-Track Buildings

As shown in Fig. 16, the horizontal vibration response of different building functional areas are compared, including the vibration acceleration and the VL_{zmax} of the office building (mid-span point "O1", side wall point "O2", corner point "O3"), the residential building (near track point "R1", far track point "R2"), and the parking garage (column point "P1", mid-span point "P2").

From the comparison data, compared with the side wall point "O2" and the corner point "O3", the vibration of the office building at the mid-span point "O1" is the largest, the reason is that there is vibration wave energy superposition

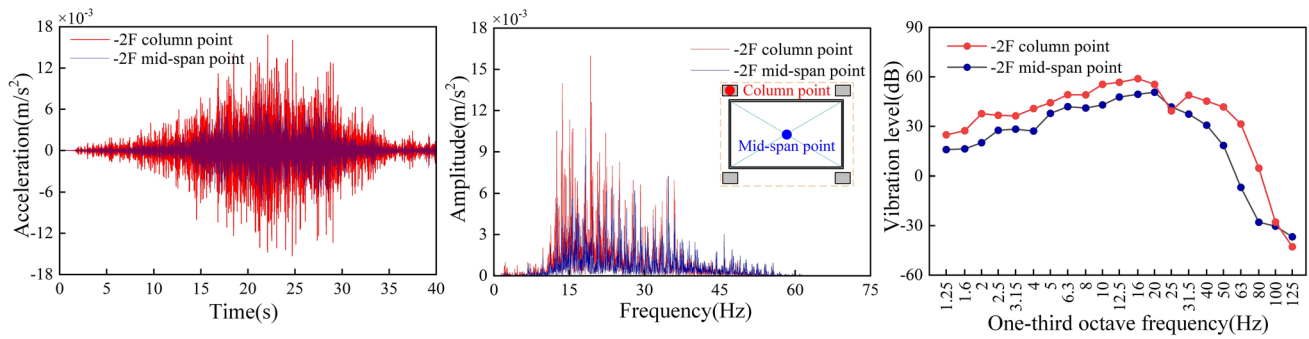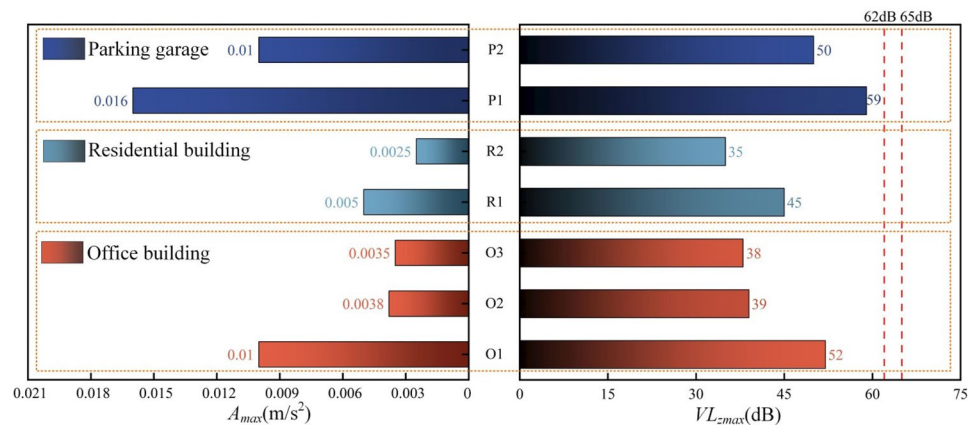**Fig. 14** Comparison of horizontal vibration of residential building

Fig. 15 Comparison of horizontal vibration of parking garage

Fig. 16 Comparison of horizontal vibration of over-track buildings

at the mid-span point. The horizontal vibration level of the parking garage in the over-track buildings is the largest, the VL_{zmax} of the parking garage is 59 dB, and the vibration of the column point "P1" is larger than that of the mid-span point "P2". The vibration acceleration of near track point "R1" is larger than that of "R2" away from the track, and the VL_{zmax} is 10 dB different.

5 Vertical Vibration of Over-Track Buildings

This chapter studies the vibration level of the office building, residential building, and parking garages, respectively, and the vibration propagation law between different floors is analyzed.
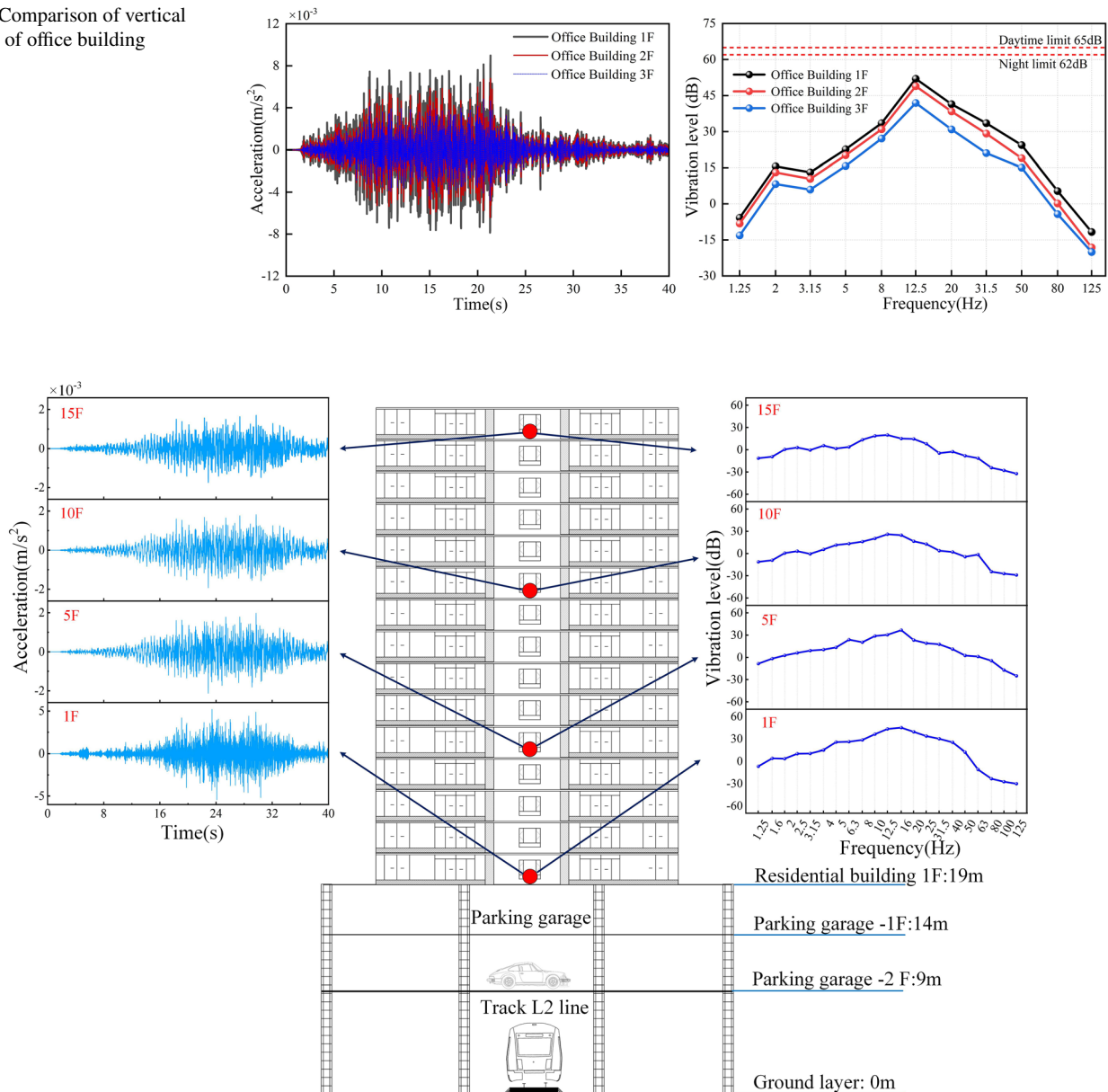
5.1 Vertical Vibration of Office Building

The above research shows that the vibration level of the office building's mid-span point is larger than that of the side wall point and the corner point, and the vibration of the mid-span position is analyzed in depth in Fig. 17. The mid-span positions acceleration of the 1st, 2nd, and 3rd floors are selected, respectively. With the rise of the floor, the

acceleration amplitude is decreasing, and the peak acceleration of the first floor is 0.01 m/s². The vibration acceleration waveform characteristics of each floor are similar, and the whole is fusiform. The VL_{zmax} from the first floor to the third floor are 52.02, 49.95, and 42.94 dB, respectively. Based on the above standards, according to the standard of "resident, cultural and educational area", the office building is limited to 62 dB at night and 65 dB during the day, and the vibration response of the office building is within the standard limit.

5.2 Vertical Vibration of Residential Building

As shown in Fig. 18, the vibration acceleration of the mid-span point on the 1st, 5th, 10th, and 15th floors of the residential building are extracted, respectively.

From the time domain, the peak acceleration of the 1st floor is 0.002 m/s², and with the increase of residential floors, the acceleration presents nonlinear attenuation. This is because the vibration wave mainly propagates through the bearing column, the bearing column structure has a large density and high strength, and vibration energy is greatly attenuated at the lower floors. From the frequency domain, the main vibration frequency is in the range of 10–20 Hz, and the vibration acceleration level is

Fig. 17 Comparison of vertical vibration of office building

Fig. 18 Vertical vibration of residential building

concentrated in 25–45 dB. The vertical vibration propagation distance is proportional to the vibration energy attenuation.

As shown in Fig. 19, to better show the vertical vibration transmission law of the residential building, the VL_{zmax} of the residential building is analyzed according to the simulation results, and the VL_{zmax} fitting curve is drawn. It can be seen that the VL_{zmax} attenuates rapidly in the lower floors of residential buildings. As the floor rises, the VL_{zmax} attenuates slowly, showing an exponential attenuation trend, and the VL_{zmax} attenuates by 20 dB. The VL_{zmax} fit curve formula is as follows:

$$Z = 26.3 * \text{EXP}(-F/3.2) + 25.6 \tag{8}$$

In the equation, Z is the VL_{zmax} of the residential building, F is the number of floors, and EXP is an exponential function based on the natural constant "e".

5.3 Vertical Vibration of Parking Garage

The above analysis shows that the column point of the office building has a larger vibration than that of the mid-span
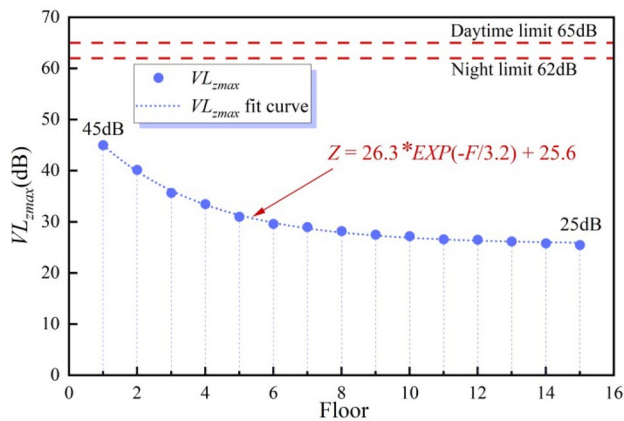
Fig. 19 The VL$_{zmax}$ fit curve of residential building

point. The vibration characteristics of the column point are further analyzed in the parking garage, as shown in Fig. 20.

The acceleration spectrum of the negative first floor is close to that of the negative second floor in the frequency distribution, and the VL$_{zmax}$ of the parking garage is 59 dB.
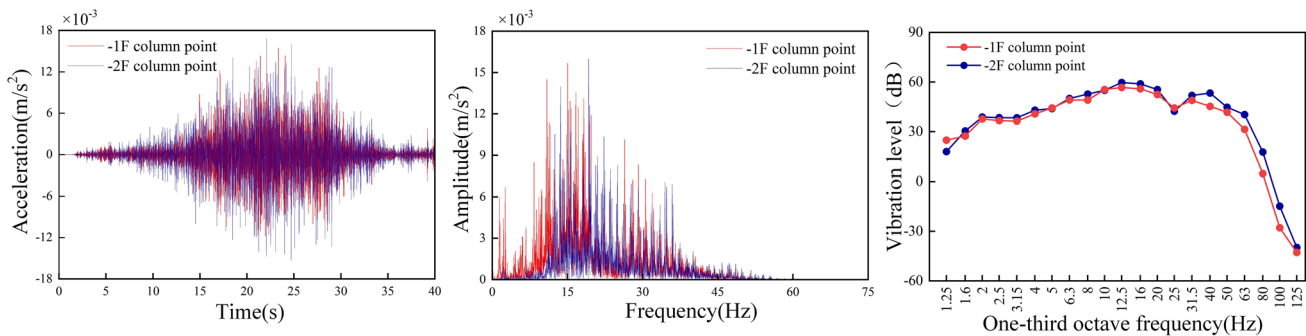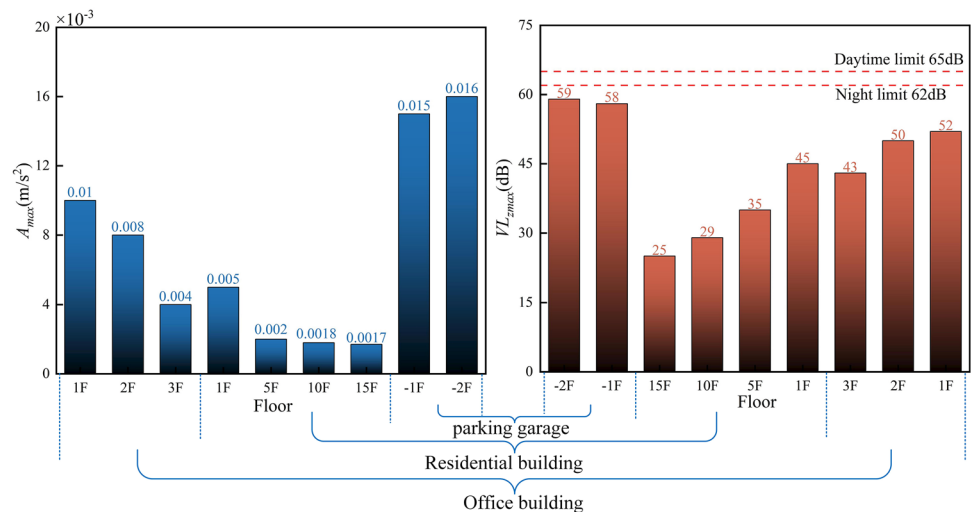
The acceleration of the double-layer parking garage at the mid-span point is propinquity, and the acceleration waveform characteristics are similar. The vertical vibration of the parking garage is no vibration exceeding the standard limit. Due to the large number of bearing columns in the parking garage and the higher structural strength, the rigid connection of the two floors is large, resulting in the vibration level of the upper and lower parking garages being similar.

5.4 Comparison of Vertical Vibration of Over-Track Buildings

The peak acceleration and the VL$_{zmax}$ of the office building, residential building, and parking garage are listed, respectively, as shown in Fig. 21. The vibration acceleration of the low floor attenuates rapidly, and the vibration acceleration of residential buildings shows an exponential attenuation trend with the rise of floors. The vibration of residential buildings is slightly smaller than that of office buildings. The overall vertical vibration of the parking garage is larger than that of the office building and the residential building. The reason

Fig. 20 Comparison of vertical vibration of parking garage

Fig. 21 Comparison of vertical vibration of over-track buildings

is that the parking garage is closer to the track L2 line, and the vibration energy is concentrated on the bottom floor.

6 Conclusions

Aiming at the issue of the over-track buildings low-frequency vibration caused by metro operation in southwest China, combining numerical simulation with field test is adopted, considering the influence of the collision between the metro wheelset and the turnout switch rail, comparing the vibration differences between the non-turnout area and the turnout area, and the vibration response of parking garages, office building, and residential building are further studied, respectively. The conclusions can be obtained as follows:

(1) The vibration response of different test points is analyzed by field test, the vibration energy attenuation along the track direction is slow, and the vibration response of the throat area is extensively greater than that of the parking area.
(2) As the vibration wave is delivered to the over-track buildings, the vibration energy of the low-rise building decays faster, and the over-track buildings are mainly low-frequency vibrations. The main vibration frequency of office building is concentrated in 10–20 Hz. The larger the room area, the easier it is to cause floor vibration.
(3) The main vibration frequency of the residential building is similar to that of the office building, and the VL_{zmax} is 45 dB. Due to the superposition of office building vibration energy in the same room, the vibration response of the mid-span point is obviously greater than that of the corner point and the side wall point. The vertical and horizontal vibration levels of the over-track buildings show a decreasing trend.
(4) The vibration level of the parking garage is larger than that of other buildings. The vibration acceleration level near 12.5 Hz in the parking garage is on the verge of exceeding the standard limit, and the vibration response of the column point exceeds that of the mid-span point in the parking garage. The rigid connection of the two floors is larger in the parking garage, so the floor vibration levels of the upper and lower parking garages are close to each other. (5) The numerical results in this paper can provide data support for the vibration control of over-track buildings above the metro depot. The vibration of the over-track buildings is within the standard limit range, but the limit of the secondary structural noise is more stringent. Subsequent studies will consider the introduction of secondary structural noise.

(5) The numerical results in this paper can provide data support for the vibration control of over-track buildings above the metro depot. The vibration of the over-track buildings is within the standard limit range, but the limit of the secondary structural noise is more stringent. Subsequent studies will consider the introduction of secondary structural noise.

Author Contributions All authors contributed to the study theories and methods. The first draft of the manuscript was written by Fangshuang Wan. Materials preparation and data collection and analysis by Zhaowei Chen, Fangshuang Wan, and Chunyan He. All authors revised and approved the final manuscript.

Declarations

References

1. Ma LX, Liu WN, Liu WF et al (2016) Sliced finite element-infinite element coupling model for predicting environmental vibration induced by metro train. Chin J Rock Mech Eng 35(10):2131–2141 (**in Chinese**)
2. Liang RH, Ding DY, Cheng YL et al (2022) Experimental study of the source and transmission characteristics of train-induced vibration in the over-track building in a metro depot. J Vib Control 29(7–8):1738–1751
3. Chen YM, Feng QS, Liu QJ et al (2021) Experimental study on the characteristics of train-induced vibration in a new structure of metro depot. Environ Sci Pollut Res 28(30):41407–41422
4. Zhang XH, Zhou SH, He C et al (2021) Experimental investigation on train-induced vibration of the ground railway embankment and under-crossing subway tunnels. Transp Geotech 26:100422
5. Zhang ZS, Gao M, Song J et al (2021) Duxseal as backfill material for subway lining to mitigate railway vibrations: field experiments. Transp Geotech 30:100607

6. Shao ZP, Bai W, Dai JW et al (2023) Monitoring and analysis of railway-induced vibration and structure-borne noise in a transit oriented development project. Structures 57:105097

7. Di HG, Su GB, Yu JY et al (2023) Field measurement and evaluation of vibrations inside buildings above metro tunnels. Soil Dyn Earthq Eng 166:107767

8. Cao ZL, Guo T, Zhang ZQ et al (2018) Measurement and analysis of vibrations in a residential building constructed on an elevated metro depot. Measurement 125:394–405

9. Tao ZY, Zou C, Wang YM et al (2021) Vibration transmissions and predictions within low-rise buildings above throat area in the metro depot. J Vib Control 29(5–6):1105–1116

10. Zhang ZJ, Li XZ, Zhang X et al (2022) Semi-analytical simulation for ground-borne vibration caused by rail traffic on viaducts: vibration-isolating effects of multi-layered elastic supports. J Sound Vib 516:116540

11. Chen J, Geng JL, Gao GY et al (2022) Mitigation of subway-induced low-frequency vibrations using a wave impeding block. Transp Geotech 37:100862

12. Ling YH, Zhang YZ, Luo Q et al (2023) Field measurement and simplified numerical model for vibration response of subway superstructure. Structures 47:313–323

13. Xiong YL, Zhang SL, Wu ZZ et al (2020) Comparative analysis of the influence of building vibration on human comfort caused by blasting and subway train loads. Environ Earth Sci 455:012160

14. Zou C, Wang YM, Zhang X et al (2020) Vibration isolation of over-track buildings in a metro depot by using trackside wave barriers. J Build Eng 30:101270

15. Ling YH, Gu JX, Yang TY et al (2019) Serviceability assessment of subway induced vibration of a frame structure using FEM. Struct Eng Mech 71:131–138

16. Chen X, Xiong ZM, Zhuge Y et al (2023) Numerical analysis on the seismic performance of subway station in ground crack area. Tunn Underg Space Technol 134:105012

17. Kouroussis G, Vogiatzis K, Connolly D et al (2018) Assessment of railway ground vibration in urban area using in-situ transfer mobilities and simulated vehicle-track interaction. Int J Rail Transp 6(2):113–130

18. Cao R, Ma M, Sun X et al (2023) Transmission characteristics of train-induced vibration in buildings based on wave propagation analysis. Constr Build Mater 378:131154

19. Mouzakis C, Vogiatzis K, Zafiropoulou V (2019) Assessing subway network ground borne noise and vibration using transfer function from tunnel wall to soil surface measured by muck train operation. Sci Total Environ 650(2):2888–2896

20. Wang S, Xin T, Wang PS et al (2023) Novel method for obtaining transfer characteristics of subway-induced ground vibrations. Int J Mech Sci 255:108462

21. Li WB, Liu WF (2023) A novel formulation for transfer path identification and vibration prediction in the over-track building induced by trains. Environ Sci Pollut Res 30(18):52732–52748

22. Ma M, Jiang BL, Liu WF et al (2020) Control of metro train-induced vibrations in a laboratory using periodic piles. Sustainability 12(14):5871

23. Tao ZY, Wang YM, Sanayei M et al (2019) Experimental study of train-induced vibration in over-track buildings in a metro depot. Eng Struct 198:109473

24. Zhai WM (2014) Vehicle-track coupled dynamics, 4th edn. China Railway Press

25. Chen ZW, Peng S, Zeng DF et al (2023) Basement design for vibration reduction of high-rise buildings under Metro Operation. KSCEJ Civ Eng 27:1732–1750

26. Ma QT, Wang K, Wang X et al (2023) Numerical and experimental investigation of longitudinal rail creep at turnouts on steep ramps under repeated loads considering realistic braking loads of vehicles. Eng Fail Anal 151:107380

27. Chen ZW, Zhu G (2021) Dynamic evaluation on ride comfort of metro vehicle considering structural flexibility. Arch Civ Mech Eng 21(4):162

28. Zhai WM, Xia H, Cai CB et al (2013) High-speed train-track bridge dynamic interactions part I: theoretical model and numerical simulation. lnt J Rail Transp 1(1/2):3–24

29. Yang WG, Li H, Xi JK (2019) Analysis of subway induced vibration of a modern building and research on vibration reduction and isolation measures. J Vib Eng Technol 36(01):147–158 (**in Chinese**)

30. Liu JB, Du YX, Du XL et al (2006) 3D viscous-spring artificial boundary in time domain. Earthq Eng Eng Vib 5:93–102